Deanship of Graduate Studies

AL-Quds University

Double-Hump Distribution in the Polar Wind

By

Samer M. Hajiji

M.Sc. Thesis

2004

Double-Hump Distribution in the Polar Wind

By

Samer M. Hajiji

(B.Sc. in Physics, Bir Zeit University)

Supervised by:

Imad A. Barghouthi, Ph.D.
Saker Darwish, Ph.D.

"Thesis Submitted to the Graduate college in Partial Fulfillment of the Requirement for the Degree of Master of Science in Physics"

Jerusalem, Al-Quds University

Palestine

June, 2004

Deanship of Graduate Studies
Program of Postgraduate Studies in Physics

Double-Hump Distribution in the Polar Wind

Student Name: Samer M. Hajiji

Registration No.: 9910893

Thesis submitted for examination on June 1, 2004 and accepted by the examining committee formed of the following:

Committee members		Signature
1-Dr. Imad A. Barghouthi.	(Chairman)	----------
2- Dr. Saker Darwish.	(Internal Examiner)	----------
3- Dr. Mohammad M. Abu-Samreh.	(Internal Examiner)	----------
4- Dr. Esma'el Badran.	(External Examiner)	----------

Declaration

I certify that this thesis submitted for the degree of Master of physics is the result of my own research, except where otherwise acknowledged, and that this thesis (or any part of the same) has not been submitted for a higher degree to any other university or institution.

(Signed: _____)

Samer Mohammed Abdelghany Hajiji

Date: June 1, 2004.

Acknowledgement

After thanking Allah, who granted me to complete this work, I would like to express my thanks to my supervisor, Dr. Imad Barghouthi for his help and support during all phases of this work. I would like also to acknowledge my co-supervisor Dr. Saker Darwish for his support, special thanks with respect to my parents, for the encouragement and support, to my brothers and to my sisters. Very special thanks go to my wife, Ebtihaj, and to my daughters Lara and Sara, for the love and encouragement. I would like to express my thanks to my classmates, especially, my friends Muayad Alhih and Muthaffar Atout, for the unlimited assistance.

Dedication

To my father, Abu Samer, my mother, Um Samer.

To my wife, Ebtihaj, and my daughters, Lara and Sara.

To my brothers, and my sisters.

With Admiration

Abstract

In this study, the Monte Carlo model was used to investigate the characteristics of the H^+ polar wind under the effects of gravity, divergence of magnetic field , polarized electric field, Coulomb collision of H^+-O^+, and wave-particle interaction (WPI). The Fokker-Planck representation for Coulomb collision was used, and the wave-particle interaction was considered as a diffusion in velocity space. The simulation region was extended from 230 Km to 5350 Km.

It was found that WPI plays an important role in the characteristics of the H^+ polar wind. It enhances and increases the drift velocity, parallel temperature and perpendicular temperature of the H^+ ions; while it decreases the density. The WPI results in changing the shape of the velocity distribution function rapidly for high WPI values.

The H^+ double-hump distribution was observed at intermediate altitudes or around (~1570 km). Besides, this study has shown that the formation of H^+ double hump distributions can be observed at lower altitudes, (namely; ~1030 km for $\widetilde{D}_\perp = 0.01$ and at ~890 km for $\widetilde{D}_\perp = 0.1$) when WPI is included.

ملخص

في هذه الدراسه تم استخدام تقنية المونتي كارلو لدراسة خصائص الرياح القطبيه لايونات الهيدروجين تحت تاثير الجاذبيه الارضيه، انحراف خطوط المجال المغناطيسي الارضي، المجال الكهربائي المستقطب، اثر كولومب على تصادمات ايونات الهيدروجين وايونات الاكسجين وتفاعلات الموجه-الماده، تمتد منطقة الدراسه من ارتفاع 230 كم الى ارتفاع 5350 كم، وقد تم استخدام نموذج فوكر-بلانك لدراسة تاثير كولومب على تصادمات الانويه وتم اعتبار تفاعل الموجه-الماده كانتشار في فضاء السرعة.

من خلال الدراسة وجد أن تفاعل الموجه-الماده تلعب دورا هاما في خصائص الرياح القطبيه لتوزيع ايونات الهيدروجين، حيث تعمل على زيادة السرعة الاندفاعيه،وعلى زيادة عزم درجة الحرارة الموازية، و عزم درجة الحرارة العمودية لايونات الهيدروجين، بينما تقل الكثافة. اما شكل اقتران توزيع السرع فوجد انه يتغير باضطراد بسبب تفاعل الموجه-الماده، و خاصة عندما تكون قيمة معامل الانتشار كبيرة.

في هذه الدراسه تم الحصول على توزيعات ثنائية القمه لايونات الهيدروجين على ارتفاعات متوسطه (~1570كم). علاوة على ذلك، فقد تميزت هذه الدراسه بالحصول على توزيعات ثنائية ألقمه لايونات الهيدروجين وبالتحديد وجود هذه التوزيعات على ارتفاعات منخفضة (~1030كم عندما تكون قيمة $\widetilde{D}_{\perp} = 0.01$ ، و~890 كم عندما تكون قيمة $\widetilde{D}_{\perp} = 0.1$)كنتيجة طبيعيه لادخال اثر تفاعل الموجه-الماده.

Table of Contents

List of Figures

List of Abbreviations

WPI	Wave-particle interaction
PIC	Particle in cell
PWI	Plasma wave instrument
DE-1	Dynamic explorer-1
VDF	Velocity distribution function

Chapter One

INTRODUCTION

Chapter One

Introduction

1.1 The Polar Wind

The geomagnetic field configuration in a vast region closed to the earth is modified by the interaction of the solar wind with the earth dipole magnetic field (*Axford* and *Hines*, 1961). A typical shape of the geomagnetic field lines is shown in Figure 1. When the solar wind plasma flows a cross magnetic field lines, it compresses the magnetic field lines in the sunward side and a long tail-like structure in the antisunward side of the earth is formed(*Ganguli*, 1996). Since the pressure in the ionosphere is much greater than along the magnetosphere tail, a continual escape of thermal plasma should occur along these tails. This type of outflow was termed as "*polar wind*" in analogy to the solar wind (*Axford*, 1968). *Axford* has defined the polar wind as an outflow of thermal plasma in the polar cap region from high-latitude terrestrial ionosphere to the magnetosphere.

Sources of the polar wind are ionospheric plasma and the solar wind. In general the polar wind consists mainly of H^+, He^+, and O^+ ions and free electrons.

As the polar wind flows, four major transitions have been occurred: Firstly, chemical to diffusion dominance, secondly, heavy to light ion composition, thirdly, collision dominated to collisionless regimes and fourthly subsonic to supersonic flow (*Barghouthi et al.*, 1993). Collisions are important up to 2500 km after that a temperature anisotropy have been exhibited by the ions and electrons. Outflow of polar wind was found to vary with seasons, solar cycles and geomagnetic activities. For instance O^+ flux exhibits maximum values during summer season, while H^+ flux

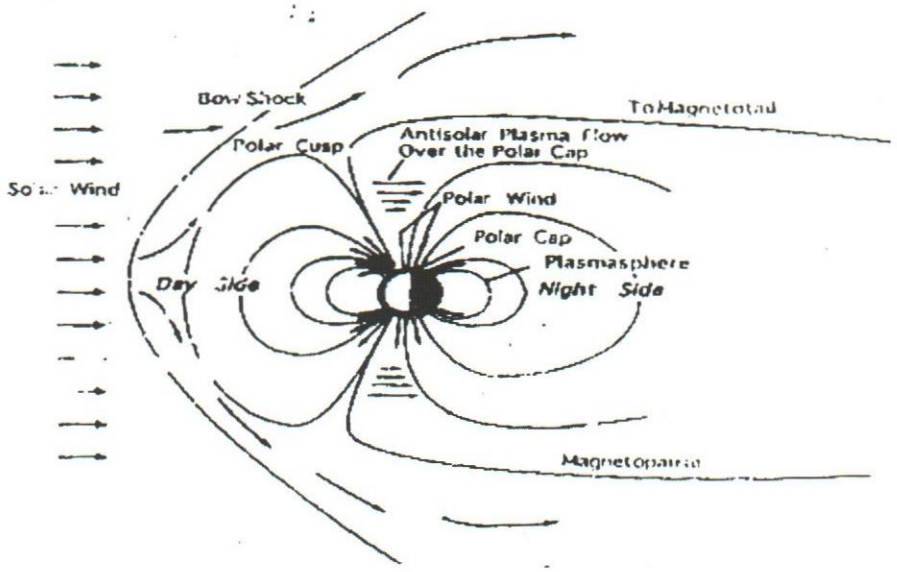

Figure 1. Schematic representation of the shape of the geomagnetic field lines and the high-altitude magnetosphere region. (*Ganguli*, 1996).

exhibits its maximum values in the spring season. Furthermore, the integrated H^+ ions flux maximum values were exhibited during the noon sector and minimum during the midnight sector (*Ganguli*, 1996).

The polar wind flows up to distances approximately several earth radii into the magnetosphere. At 800 km above the earth surface, the ion outflow becomes diffusive. At altitudes of 1500-2500 km the polar wind flow changes from collision to collisionless, where velocities change might be from subsonic to supersonic respectively, and the temperature anisotropy ($T_{\parallel}/T_{\perp}$) should be reversed.

Accordingly, regions of the polar wind are divided into dominated collision region (ion barosphere) and the collisionless region (ion exosphere). These two regions were separated by a narrow transition layer (*Barghouthi et al.*, 1993) where the four major transitions mentioned above have been occurred (see Figure 2).

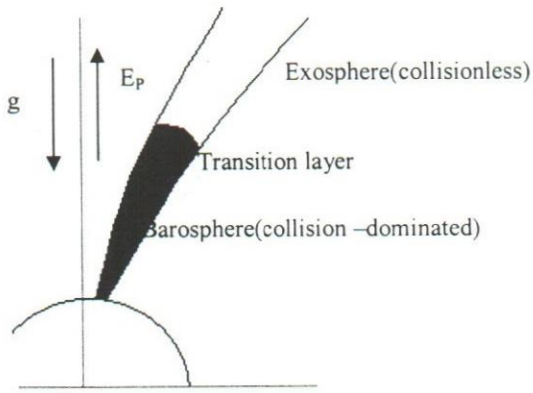

Figure 2. Schematic representation of the three regions of the polar wind. (*Barghouthi et al.*, 1993)

1.2 Previous Work

There was several models that have been introduced and developed to study the characteristics of the polar wind, the first theoretical attempt was based on solving the hydrodynamic continuity and momentum equations, and making use of the assumption that the ionosphere is isothermal (*Banks* and *Holzer*, 1968 and 1969). They found that the ampipolar electric field drives H^+ ions parallel to the geomagnetic field lines. Furthermore, the model assumed supersonic nature of the flow is included, and neglected the effects of H^+-O^+ collisions (*Holzer et al.* 1971). This guarantee heat transfer process in the hydrodynamic is included in order to study the ions temperature anisotropies.

The generalized transport model was developed to include the generalized transport equation by taking into account the velocity moments of the Boltzmann equation. A set of partial differential equations were obtained by multiplying the Boltzmann equation by a set of velocity functions and integrating over the velocity space. Obtained equations were used to describe the spatial-temporal variation of the velocity moments.

A specific form of the particle velocity distribution function must be adopted in order to have a complete set of equations. The general approach is based on expanding the distribution function in terms of a complete, orthogonal series of functions using the zeroth order distribution function as the weight factor. For example, if the zeroth-order distribution function is assumed to be Maxwellian then truncations of the series at various levels lead to the well-known 5-moments, or 13-moments, and 20-moments approximations.

The first use of the generalized transport model was based on modeling the subsonic polar wind outflow using the coupled steady state 13-moments system of transport equations for H^+, O^+ and e^- plasma from 1,200 km to 12,000 km, the number of moments was reduced from 13 to 5 moments (*Schunk* and *Watkins*, 1981). The 5 moments are: the density, the field aligned velocity, the temperature parallel and perpendicular to the geomagnetic field lines, and the heat flow (*Ganguli*, 1996).with a proper choice of the base function and the correction terms, the model can be used to study all the three polar wind regions (*Barakat et al.*, 1995).

On one hand, the kinetic approach was used to solve the Boltzmann equation for collision dominated plasma; on the other hand, Vlasov equation was used to solve the collisionless plasma directly in order to give the spatial-temporal variation of the particle distribution function in terms of the known distribution function at the boundary. Description of the collisionless region of the polar wind was successfully investigated using kinetic approach (*Dessler* and *Cloutier,* 1969). In this approach the result is sensitive to the assumptions made about the particle dynamics and populations. Based on the semikinetic model, H^+ has shown a near-to-Maxwellian distribution at low altitudes (*Barakat* and *schunk*, 1983). At higher altitudes (>5 R_e), the H^+ developed

a large temperature anisotropy ($T_{\parallel} > T_{\perp}$) and an upward heat-flow components (*Barghouthi et al.*, 1998).

Generally speaking, transport models neglect the effect of the wave-particle interaction (WPI) on plasma outflow. Accordingly, several linear stability studies and particle in cell (PIC) simulations have shown that the polar wind plasma became unstable. Moreover, a significant level of electromagnetic turbulence occurs above the polar cap has been observed, it was pointed out that the effect of WPI on the plasma outflow can be significant and should be included in the polar wind models (*Barakat* and *Barghouthi*, 1994a,b). The most suitable candidate model to include the WPI is the Monte Carlo model.

The Monte Carlo technique has been widely used in space physics by several authors *Barakat* and *Schunk* (1983), *Barakat* and *Lemaire* (1990), *Barakat et al.*(1995), *Barakat and Barghouthi* (1994a,b), *Barghouthi et al.*(1993, 1998, 2001 and 2003).

To study the characteristics of the polar wind, one has to calculate the velocity distribution function of the species and its velocity moments (e.g. density, drift velocity, temperature, heat flux, etc.). The corner stone is to start with the Boltzmann equation. Thus

$$\frac{\partial f_s}{\partial t} + v_s . \vec{\nabla} f_s + \left(\vec{g} + \frac{e_s}{m_s} (\vec{E} + \frac{1}{c} v_s \times \vec{B}) \right) . \vec{\nabla}_{v_s} f_s = \frac{\delta f_s}{\delta t} \qquad (1.1)$$

Where $\vec{g}$ is the gravitational acceleration e_s, m_s are the charge and mass of the species s respectively, $\vec{E}$ is the electric field, $\vec{B}$ is the magnetic field, c is the speed of light, $\vec{\nabla}$ is the space gradient, and $\vec{\nabla}_{v_s}$ is the velocity gradient. The right-hand side represents the rate of change of f_s in a given region of phase-space resulted from the collision between species (or the collision term) (*Barghouthi et al.*, 1993).

The Monte Carlo simulation has been used to study the steady flow of the H^+ ions through a background of O^+ ions, which has a local Maxwellian distribution that depends on the altitude (*Barghouthi et al.*, 1993). The simulation region was extended to include the three polar wind regions: the collision dominated, the collisionless and the transition layer. The effects of gravity, the polarization electric field, the divergence of the geomagnetic field lines, and the H^+-O^+ collisions have been included. The Fokker-Planck expression that have been used to represent H^+-O^+ Coulomb collisions can be written as (*Barghouthi et al.*, 1993)

$$\frac{\delta f_s}{\delta t} = \sum_t \int d^3 v_t d\Omega g_{st} \sigma_{st}(g_{st}, \theta)[f_s' f_t' - f_s f_t] \tag{1.2}$$

where $d^3 v_t$ is the velocity-space volume element of species t, g_{st} is the relative velocity of the colliding particles s and t, $\sigma_{st}(g_{st}, \theta)$ is differential scattering cross section, θ is the scattering angle, $d\Omega$ is the element of solid angle in the s particle reference frame, and the prime quantities represent quantities that have been evaluated after collision. One of the investigations was aimed on calculating the H^+ velocity distribution function, $f(H^+)$, and its moments. The results obtained were significant (*Barghouthi et al.*, 1993). For example, the transition layer was found to play an important in the behaviour of the H^+ flow. In the transition layer, the shape of H^+ distribution function changes rapidly in a complicated manner from Maxwellian in the barosphere to Kidney bean in the exosphere. Furthermore, the flow changes from subsonic to supersonic within the transition region, and the H^+ parallel and perpendicular temperature increase with altitude in the barosphere due to frictional heating, while decrease with altitude in the exosphere due to adiabatic cooling. Both parallel and perpendicular temperatures reach their maxima in the transition region. Moreover, the heat fluxes of parallel and perpendicular energies are positive and increase with altitude in the barosphere. They

were also found to change rapidly from their maximum (positive) to their minimum (negative) values within the transition region.

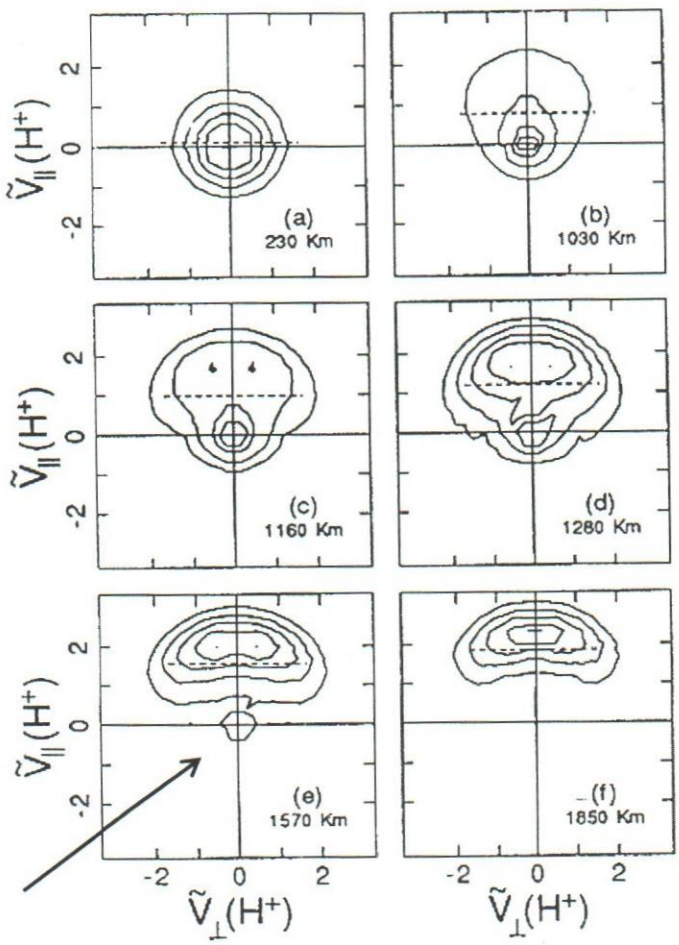

Figure 3. H^+ velocity distribution function for six altitudes, one in the barosphere, and five in the transition layer, $f(H^+$ is represented by equal value contours in the normalized velocity $(\tilde{v}_{\parallel}(H^+), \tilde{v}_{\perp}(H^+))$, where $(\tilde{v}(H^+) == v(H^+)/\left[2kT(O^+)/m(O^+)\right]^{1/2}$. The contour levels are at $0.9\, f_{max}$, $0.8\, f_{max}$, $0.7\, f_{max}$, etc., where f_{max} is the maximum value of $f(H^+)$. (*Barakat et al.*, 1995).

The model has been modified to include collisions and the effects of body forces such as: gravity, magnetic field and electric field. These effects can alter the results significantly.

The characteristics of the H^+ polar wind, using the Monte Carlo simulation has been used to study the steady state flow of H^+ ions (*Barakat et al,* 1995) through a background of O^+ ions. Effects of the diverging of geomagnetic field lines, the gravitational force, the electrostatic field, and H^+-O^+ collisions have been included. Their study has covered the three polar wind regions in their simulation domain. The velocity distribution function of H^+ was found to be close enough to Maxwellian at low altitudes. As the ions were drifted to higher altitudes, $f(H^+)$ formed an upward tail. In the transition layer, the upward tail evolved into a second peak with Kidney bean shape and hence, $f(H^+)$ developed a double-humped shape (Figure 3).

Special attention has been focused on the details of the behaviour of $f(H^+)$ in the transition region and its close relationship to the rapid change in the heat flux. They have attributed these features to the interplay between the body forces and the velocity dependence of the H^+-O^+ Coulomb collision. The formation of the double hump was found to have several important consequences, even though a direct observation of such a distribution may not be feasible with the existing technology.

Barghouthi et al. (2001) have used Monte Carlo simulation to study the effects of Kappa H^+ distribution on the H^+ outflow in the polar wind. They have considered the effects of gravity, the polarization electric field, the divergence of the geomagnetic field lines and Coulomb collision of the H^+ - O^+ in a background of O^+ ions. The difference between the Monte Carlo simulation presented in *Barakat et al.*(1995) and *Barghouthi et al.*(2001)is in the choice of the distribution function at low altitude boundary. *Barghouthi et al.*(2001)have used a Kappa distribution (a distribution that has suprathermal tails) for the H^+ distribution function, while *Barakat et al.*,(1995) have used Maxwellian distribution. They have found that suprathermal particles are very important in modelling the polar wind velocity distribution function.

Barakat and *Barghouthi* (1994a) have developed a Monte Carlo simulation to study the effects of wave-particle interaction on the H^+ and O^+ outflow in the polar wind. The simulation region was extended from the exobase 1.7 R_E to 10 R_E. They have considered also geomagnetic field that is proportional to r^{-3}, where r is the geocentric distance, and the distribution function was assumed to be a drifting Maxwellian one in the exobase. Furthermore, the electrostatic and gravitational potentials was assumed to have the following form

$$\Phi(r) = \frac{kT_e}{e} \ln\left(\frac{n_e}{n_{eo}}\right) + GM_e\left(\frac{1}{r_o} - \frac{1}{r}\right) \tag{1.3}$$

where k is the Boltzmann's constant, T_e is the electron temperature, n_e and n_{eo} are the electron densities at r and r_0 respectively, G is the universal gravitational constant and M_E is the mass of the earth. The effect of WPI was included in terms of the quasi-linear velocity diffusion rate perpendicular to the geomagnetic field as:

$$D_\perp = \frac{\eta q_j^2}{4m_j^2} |E(\omega = \Omega)|^2 \tag{1.4}$$

where q_j and m_j are the ion charge and mass, respectively, the ion gyrofrequency is Ω, $|E|^2$ is the spectral wave density, η is proportion of this density that corresponds to the left polarized component, and the subscript j denote the type of the species..

The normalized velocity diffusion rate was defined as (*Barakat* and *Barghouthi*, 1994a, b):

$$\tilde{D}_{\perp j} = 0.5 D_\perp r_0 \left(\frac{m_j}{2kT_{0j}}\right)^{-3/2} \tag{1.5}$$

Where T_{oj} is the "Maxwellian" temperature at the exobase, and the perturbation of the ion perpendicular velocity $\Delta v_\perp$ due to WPI was given by

$$\left\langle (\Delta v_\perp)^2 \right\rangle = 4 D_{\perp WPI} \Delta t \tag{1.6}$$

The effect of the WPI was found to be more pronounced at higher altitudes where large anisotropy predicted, by the semi-kinetic model, to occur at high altitude is reduced even for small diffusion coefficient ($\widetilde{D}_{\perp}(H^{+}) = 0.01$). As $\widetilde{D}_{\perp}(H^{+})$ increases, the temperature anisotropy is reduced and even reversed, and the H^{+} distribution function showed conic features at high altitudes for the case of strong WPI. Increasing $\widetilde{D}_{\perp}(H^{+})$, $n(H^{+})$ decreases, and $u(H^{+})$ increases such that the escape flux remains constant. Moreover, increasing $T_{\perp}(H^{+})$, and decreasing $T_{\parallel}(H^{+})$ followed by increasing at high altitudes due to the interplay between the parallel adiabatic cooling and the transfer of energy from the perpendicular to the parallel direction due to perpendicular adiabatic cooling. The lower-order moments such as $n(H^{+})$ and $u(H^{+})$ are less sensitive to the WPI than the higher-order moments such as $T_{\parallel}(H^{+})$ and $T_{\perp}(H^{+})$.

Barakat and *Barghouthi* (1994a, b) have extended their investigations to include the effects of WPI on the O^{+} outflow using Monte Carlo simulation. The results obtained for the moments of the distribution function of O^{+} was similar to that obtained for H^{+} in *Barakat* and *Barghouthi* (1994a) but an interesting phenomena was observed, "the pressure cooker effect". In this effect the WPI results in trapping some ions between magnetic and gravitational reflecting points, and consequently the ions energy is greatly enhanced.

Barghouthi et al. (1998) have extended the study to include effects of altitudes dependent WPI on the H^{+} and O^{+} polar wind. The values of $\widetilde{D}_{\perp}$ inserted in their Monte Carlo code were computed from the wave spectral density (ρ) observed by the Plasma Wave Instrument (PWI) on board Dynamic Explorer-1 (DE-1), and these values were altitude dependent. However, in previous studies, the used values of $\widetilde{D}_{\perp}$ were taken to

be constant along the simulation region. It has been shown that the plasma behaviour depends qualitatively on the details of the heating rate profile, as in the O^+ escape flux that was mainly controlled by the heating rate at low altitudes.

1.3 The Problem

Barghouthi et al.(1993) had studied the effects of Coulomb collision on the H^+ outflow and neglected the wave particle interaction. The effect of WPI on the H^+ polar wind was investigated by *Barghouthi* et al., (1998) in the absence of coulomb collisions. Effects of external forces, gravitational, electrostatic polarization and divergence of geomagnetic field were implemented in both studies.

In this study, we shall examine the effects of Coulomb collisions, WPI, gravity, electric field, and geomagnetic field altogether on the H^+ polar wind.

In other words, we shall combine *Barghouthi et al.* work in 1993 to the work in 1998 to produce a new transport equation in which all mentioned effects were included. This new equation will be used to calculate the H^+ velocity distribution function, H^+ density, H^+ drift velocity, and H^+ temperature at different altitudes. Also, the study will be extended to include the effect of WPI on the formation of the double-hump velocity distributions in the polar wind.

Chapter Two

THEORETICAL BACKGROUND

Chapter Two

Theoretical Background

2.1 Introduction

Once the distribution function is calculated, the physics about the species of interest could be known, for example: density, drift velocity, parallel and perpendicular temperatures, parallel and perpendicular fluxes.

2.2 The Boltzmann Equation

As mentioned earlier, the plasma of the polar wind consists of several species namely H^+, O^+, He^+ and e^-. In order to study the characteristics of a given species one has to find the velocity distribution function (f_s) of the nominated species. This distribution is defined as the number of species at time t having position between $\vec{r}$ and $\vec{r}+d\vec{r}$ and velocities between $\vec{v}_s$ and $\vec{v}_s+d\vec{v}_s$. The time evolution of the H^+ distribution function (which is the species of interest here) can be formulated according to Boltzmann equation as:

$$\frac{\partial f_{H^+}}{\partial t}+\vec{v}_{H^+}.\vec{\nabla} f_{H^+}+\left(\vec{g}+\frac{e_{H^+}}{m_{H^+}}(\vec{E}+\frac{1}{c}\vec{v}_{H^+}\times\vec{B})\right).\vec{\nabla}_{v_{H^+}} f_{H^+}=\left(\frac{\delta f_{H^+}}{\delta t}\right)_{coll}+\left(\frac{\delta f_{H^+}}{\delta t}\right)_{WPI} \qquad (2.1)$$

where $\vec{g}$ is the gravitational acceleration, e_{H^+}, m_{H^+} are the charge and the mass of the H^+ ion respectively. $\vec{E}$ is the electric field, $\vec{B}$ is the magnetic field, c is the speed of light, $\vec{\nabla}$ is the gradient, $\vec{\nabla}_v$ is the velocity space gradient. The left hand side of equation 2.1 represents the total change of the distribution function in a given phase-space as a result of external forces, while the left hand side represents the time rate of change of

the distribution function as a result of interactions, the interactions that are important in this study are Coulomb collisions and Wave-particle interaction, so, $\left(\frac{\delta f_{H^+}}{\delta t}\right)_{WPI}$ represents the rate of change of f_{H^+} in a given region of phase-space as a result of WPI, $\left(\frac{\delta f_{H^+}}{\delta t}\right)_{coll}$ represents the time rate of change of f_{H^+} in a given region of phase-space as a result of collisions, and is given by the Boltzmann collision term.

$$\frac{\delta f_s}{\delta t} = \sum_t \int d^3 v_t d\Omega g_{st} \sigma_{st}(g_{st}, \theta)[f_s' f_t' - f_s f_t] \tag{2.2}$$

where $d^3 v_t$ is the velocity-space volume element of species t. This represents the target background ion with which the source ion collides. The symbol g_{st} represents the relative velocity of the colliding particles s and t, $\sigma_{st}(g_{st},\theta)$ is the differential scattering cross section, θ is the scattering angle, $d\Omega$ is the solid angle element in the s particle reference frame. The prime quantities denote all quantities evaluated after collision.

The moments of the distribution function are given by

$$n_s = \int f_s(v_s) d^3 v_s$$

$$u_s = \frac{\int v_{lls} f_s(v_s) d^3 v_s}{\int f_s(v_s) d^3 v_s}$$

$$T_{\|s} = \frac{\frac{m_s}{k} \int (v_{\|s} - u_s)^2 f_s(v_s) d^3 v_s}{\int f_s(v_s) d^3 v_s}$$

$$T_{\perp s} = \frac{\frac{m_s}{2k} \int v_{\perp}^s f_s(v_s) d^3 v_s}{\int f_s(v_s) d^3 v_s} \tag{2.3}$$

$$Q_{\parallel s} = \frac{1}{n_s}\left(\frac{m_s}{2kT_s}\right)^{3/2} \int d^3 v_s \left(v_{\parallel s} - u_s\right)^3 f_s(v_s)$$

$$Q_{\perp s} = \frac{1}{2n_s}\left(\frac{m_s}{2kT_s}\right)^{3/2} \int d^3 v_s \left(v_{\parallel s} - u_s\right) v_{\perp s}^2 f_s(v_s)$$

the above quantities represent: density, drift velocity, parallel and perpendicular temperatures, parallel and perpendicular heat fluxes, respectively.

Since the plasma status show marked variation within a given region or from one region to another, and because of the mathematical difficulty associated with solving Boltzmann equation for an individual species, all trials for solving the Boltzmann equation in order to obtain the velocity distribution function have used some restrictions. Each model including hydrodynamic, kinetic, semikinetic, and generalized transport, is found to be suitable for investigating one region of the polar wind at a time and can not be applied to another region without any modifications (*Barakat et al.*, 1995).

2.2 The Coulomb Collision

In the Monte Carlo simulation, the modified transport Boltzmann model that contains the Coulomb collision has found to have a remarkable effect on the obtained results (*Barghouthi et al.*, 1993). In modified model, collision term has been modified to be the Fokker-Planck representation for Coulomb collision. In this study only the $H^+ - O^+$ collisions are taken into account, while $H^+ - H^+$ collisions are neglected. The Coulomb force between H^+ and O^+ is inversely proportional to the square of interparticle distance. For such a long-range interaction, the collision term is reduced to the following Fokker-Planck representation (*Barghouthi et al.*, 2001)

$$\frac{\partial f_s}{\partial t} = -\frac{\partial}{\partial v_s}\left(A_s f_s - \frac{1}{2}\frac{\partial}{\partial v_s} D_s f_s \right) \tag{2.4}$$

where A_s is the drag coefficient and $\ddot{D}_s$ is the diffusion coefficient tensor given by

$$\ddot{D}_s = D_{\parallel s} e_z e_z + D_{\perp s}(I - e_z e_z) \tag{2.5}$$

Generally speaking, the Coulomb collision is considered as a diffusion term in the velocity-space. In this case, the Coulomb interaction is analogous to a combination of dynamic friction corresponding to the drag term (A_s) and diffusion coefficient corresponding to the scattering of the test ions in the velocity-space $D_{\parallel s}$ and $D_{\perp s}$. The overall effect of Coulomb collision during a small time Δt (of constant drag and diffusion coefficients) is given by (*Hinton*, 1983)

$$\begin{aligned} \Delta u &= A_s \Delta t \\ \left\langle \left(\Delta v_{\parallel s}\right)^2 \right\rangle &= D_{\parallel s} \Delta t \\ \left\langle \left(\Delta v_{\perp s}\right)^2 \right\rangle &= 2 D_{\perp s} \Delta t \end{aligned} \tag{2.6}$$

Barghouthi et al. (2001) adopted the following expression for the collision frequency (τ)

$$\tau = 0.01 \frac{v_s}{A_s} \tag{2.7}$$

Where v_s is the velocity of the test ion, A_s is the drag term.

2.3 The Wave-Particle Interaction (WPI)

The interaction of ions with the ambient electromagnetic turbulence, which energizes them, has a significant influence on the plasma transport in space. *Barakat* and *Barghouthi* (1994a) have shown that the Wave-particle interaction plays a vital role in the H^+ polar wind. *Barakat* and *Barghouthi* (1994b) have used Monte Carlo technique to include the effects of WPI on the O^+ polar wind.

Barghouthi et al.(1998) had considered the wave-particle interaction dependence on altitude and its effects on the polar wind had been investigated. In their study, the interaction between ions and the electromagnetic cyclotron waves of ion can be described by the expression (*Hinton,* 1983*)*:

$$\left(\frac{\partial f_s}{\partial t}\right)_{WPI} = \left(\frac{1}{v_\perp}\right)\frac{\partial}{\partial v_s}\left(D_{s\perp} v_\perp \frac{\partial f}{\partial v_\perp}\right) \tag{2.8}$$

where $D_{s\perp}$ is the quasi-linear velocity diffusion coefficient rate that is perpendicular to $\boldsymbol{B}$ and resulted from the WPI for the species s. The parameter $D_{s\perp WPI}$ is given by(*Hinton,* 1983*)*

$$D_{s\perp WPI} = \frac{\eta q_s^{\,2}}{4m_s^{\,2}}\left|\mathrm{E}(\omega = \Omega_s)\right|^2 \tag{2.9}$$

where q and m are the charge and mass of ions, respectively, Ω is the ion gyrofrequency, $|\mathbf{E}|^2$ is the spectral wave density and η is proportional to density that is corresponds to the left polarized component.

In this study, the effects of wave-particle interaction during the period Δt is taken into account by perturbing the ions perpendicular velocity by a random increment $\Delta v_\perp$ such that

$$\left\langle \left(\Delta v_\perp\right)^2 \right\rangle = 4\tilde{D}_{\perp WPI} \tag{1.6}$$

In the first part of this work $\tilde{D}_{\perp WPI}$ is changed parametrically and in each simulation 10^5 particles are injected one by one. Five different WPI levels are considered, $\tilde{D}_{\perp WPI}$=0.001, 0.01, 0.1, 1.0, 5.0. A specific value of $\tilde{D}_{\perp WPI}$ is used and this value is considered constant during the simulation.

For each value of $\tilde{D}_{\perp WPI}$, the velocity distribution function and its velocity moments are obtained.

Also, in the second phase of this work, we consider the $\widetilde{D}_{\perp WPI}$ to be velocity dependent according to the following formula (*Chang*, 1993):

$$\widetilde{D}_{\perp WPI} = \widetilde{D}_{\perp WPIO}\left(\frac{\widetilde{v}_{\perp}}{1+\widetilde{v}_{\perp}^{4}}\right) \tag{2.10}$$

where $\widetilde{D}_{\perp WPIO}$ values changes from 0.001 to 10.0.

The above modification will be included in the Monte Carlo model and the new model will be used to obtain H^+ velocity distribution and its velocity moments for different values of $\widetilde{D}_{\perp WPIO}$.

Chapter Three

MONTE CARLO TECHNIQUE

Chapter Three

Monte Carlo Technique

3.1 Monte Carlo Technique

3.1.1 Introduction

Monte Carlo method plays an important and powerful role in space plasma. In the Monte Carlo simulation method, we follow the motion of the particle under the effects of forces acting on it. In this study, the forces acting on the particle (H^+) are: gravity, geomagnetic field, polarization electric field, Coulomb collision and wave-particle interaction.

The simulation region extends from 230 km to about 5400 km so it includes collision dominated, transition layer and collisionless regions. The effects of body forces are calculated from the basic laws of motion and the effects of Coulomb collision as well as the WPI is represented as a diffusion in velocity space, therefore, the change in H^+ velocities is calculated easily after calculating the values of diffusion and drag coefficients. In the first part of this study, we have used parametric values for $\tilde{D}_{WPI}$, while in the second part of the study we have used the $\tilde{D}_{WPI}$ values having dependence on the test ion velocity.

The O^+ ions are considered to be in static equilibrium in all the simulation region. Consequently, their distribution function is assumed to be locally Maxwellian, such distribution depends only on the altitude and the O^+ temperature is assumed to be 2500 K. Moreover, the distribution function of H^+ is considered to be non-drifting Maxwellian at the exobase.

In this section we shall briefly describe the expression used in the Monte Carlo code. The Monte Carlo generations of the expressions in this section are given by *Barghouthi et al.*, (2003).

The distribution function of H^+ at the exobase is considered to be non-drifting Maxwellian. Thus

$$f(v) = n\left(\frac{m}{2\pi kT}\right)^{\frac{3}{2}} e^{-\frac{mv^2}{2kT}} \tag{3.1}$$

where n is the number density, k is the Boltzmann constant, T is the temperature of ions, m is the mass of the ion and v is the velocity that can be generated randomly.

Writing v^2 as $v^2 = v_{\parallel}{}^2 + v_{\perp}{}^2$, where $v_{\parallel}$ *and* $v_{\perp}$ are the velocities parallel and perpendicular to the geomagnetic field lines, we can write *f(v)* as a product of two functions $f(v) = nf(v_{\parallel})f(v_{\perp})$ with

$$f\left(v_{\parallel}\right) = \left(\frac{m}{2\pi kT}\right)^{\frac{1}{2}} e^{-\frac{mv_{\parallel}{}^2}{2kT}} \tag{3.2}$$

$$f\left(v_{\perp}\right) = \left(\frac{m}{2\pi kT}\right) e^{-\frac{mv_{\perp}{}^2}{2kT}} \tag{3.3}$$

where $f(v_{\parallel})$, $f(v_{\perp})$ are the H^+ velocity distribution function parallel and perpendicular to the geomagnetic field respectively.

3.1.2 Generation of $v_{\perp}(H^+)$

The probability density of finding an H^+ particle having perpendicular velocity $v_{\perp}$ was (*Aldrich*, 1985):

$$P(v_{\perp}) = 2\pi\, v_{\perp} f(v_{\perp}) \tag{3.4}$$

For a random perpendicular velocity, we shall use the following expression

$$\int_0^{v_\perp} p(v'_\perp)dv'_\perp = Ran \tag{3.5}$$

where *Ran* is a random number between (0,1), solving the integral we get:

$$v^2{}_\perp = -\left(\frac{2kT}{m}\right) ln(1 - Ran) \tag{3.6}$$

3.1.3 Generation of $v_\parallel$ (H^+)

Here, we our interest is focused on H^+ ions that have parallel velocities greater than zero (i.e. particles that cross the lower boundary). The probability of finding such particle with positive velocity is given by

$$p(v_\parallel) = 2\pi v_\parallel \left(\frac{m}{2\pi kT}\right) e^{-\frac{mv_\parallel^2}{2kT}} \tag{3.7}$$

again using the same procedure as in $v_\perp$, and solving the integral we get

$$v^2{}_\parallel = -\left(\frac{2kT}{m}\right) ln(1 - Ran) \tag{3.8}$$

3.1.4 Variation of Velocities due to external Forces

The external forces that we are interested in this study are: gravity, electric field and geomagnetic field, and the perturbation of the ion's velocity. Effects due to these forces in period of Δt are calculated from the classical laws of physics, as explained in the following three subsections.

3.1.4.1 Gravitational field

The gravitational force acting on a particle moving in the space of the earth is given by $F = mg$, where m is the mass of the particle and g is the gravitational field. From

Newton's universal law of gravity $F = \frac{GM_e m}{r^2}$, where G is the gravitational constant, M_e is the mass of the earth, and r is the geocentric constant, one can easily show that:

$$g = \frac{F}{m} = G\frac{M_e}{r^2} \tag{3.9}$$

where g is directed downward all the time.

The value of g is considered to be constant in the same layer, its value is calculated by finding its value at the lower and upper boundaries using equation (3.9) and then taking the average of these two values.

3.1.4.2 Polarization Electric Field

Since the mass of electrons is much less than that for ions, a slight charge separation occurs in response to gravity, with electrons tending to reside on the top of the ions. This slight separation of charge creates polarization electrostatic field, which in it's role prohibits further charge separation. After developing the electrostatic field, the electrons move together under the action of gravity, density and temperature gradients. Such motion is called ambipolar diffusion.

To describe the outflow of plasma under the effect of polarization electric field, many approximations are used for simplicity. One of these approximations is diffusion approximation, in which wave phenomena are neglected and the flow of plasma is subsonic. Also, since the ions and electrons move together, a net zero current conditions prevail. In addition, for a partially ionized plasma, the heat flow can also be ignored. Under such conditions, the momentum equation of electrons is given by (Schunk and Nagy, 2000):

$$\nabla_{\parallel} p_e + \left(\nabla . \boldsymbol{\tau}_{\mathbf{e}}\right)_{\parallel} + n_e e \mathbf{E}_{\parallel} - n_e m_e \mathbf{g}_{\parallel} = n_e m_e \upsilon_{ei} \left(\mathbf{u}_i - \mathbf{u}_e\right)_{\parallel} + n_e m_e \upsilon_{en} \left(\mathbf{u}_n - \mathbf{u}_e\right)_{\parallel} \tag{3.10}$$

where p_e is electrons partial pressure, $\mathbf{E}_{\parallel}$ is the polarization electrostatic field that develops due to the charge separation, $\boldsymbol{\tau}_e$ is electrons stress tensor, n_e is electrons density, m_e is the mass of electron, $\mathbf{g}_{\parallel}$ is the component of acceleration due to gravity along the geomagnetic field lines, υ is the collision frequency, and $\mathbf{u}_i$ and $\mathbf{u}_e$ are the drift velocity of ions and electros respectively.

However, in many applications an explicit expression for the electric field created owing to the movements of electrons is needed to get the electrostatic potential (V_E). This field can be obtained from equation (3.10). Since the mass of electron is small, the terms containing m_e can be neglected, and the electron-ion collision term can also be dropped, equation (3.10) can be written as:

$$e\mathbf{E}_{\parallel} = -\frac{1}{n_e}\nabla p_e \tag{3.11}$$

The expression is valid regardless of the number of ion species in the plasma.

For alternate form of isothermal electron gas, it is valid to write $\mathbf{E}_{\parallel} = -\nabla V_E(r)$, so equation (3.11) will be:

$$\frac{e}{kT_e}\frac{\partial V_E(r)}{\partial r} = \frac{1}{n_e}\frac{\partial n_e}{\partial r} \tag{3.12}$$

where r is the spatial coordinate either along or perpendicular to geomagnetic field ($\mathbf{B}$). To get the electrostatic potential (V_E), we integrate equation (3.12) to get the well-known Boltzmann relation:

$$n_e = n_{eo}e^{\frac{eV_E}{kT}} \tag{3.13}$$

where n_{eo} is the equilibrium electron density that prevails when $V_E = 0$. We can now write the expression of the electrostatic potential (V_E) as:

$$V_E(r) = \frac{kT_e}{e} \ln\left(\frac{n_e}{n_{eo}}\right) \tag{3.14}$$

so, the polarization electrostatic potential energy $\Phi_E(r)$ is given by:

$$\Phi_E(r) = kT_e \ln\left(\frac{n_e}{n_{eo}}\right) \tag{3.15}$$

3.1.4.3 Geomagnetic field

The magnetic field intensity results from the earth is taken to be proportional to r^{-3}, where r is the geocentric distance, so it can be written as:

$$B = \frac{B_o}{r^3} \tag{3.16}$$

where B_o is the geomagnetic field intensity at the surface of the earth.

3.1.5 The Effect of Coulomb Collision

In order to include Coulomb effect, the H^+ ions are assumed to interact with O^+ ions having a local Maxwellian distribution at equilibrium temperature T_{O^+}. Accordingly, the term of such distribution can be written as

$$f(v_{O^+}) = n_{O^+}\left(\frac{m_{O^+}}{2\pi kT_{O^+}}\right)^{\frac{3}{2}} e^{-\frac{m_{O^+}v_{O^+}^2}{2kT_{O^+}}} \tag{3.17}$$

As we did before the O^+ velocity can be generated according to

$$v_{\perp O^+} = -\left(\frac{2kT_{O^+}}{m_{O^+}}\right) ln(1 - Ran) \tag{3.18}$$

In a similar way, the $v_{\parallel\, O^+}$ distribution can be generated to represent the whole distribution function (i.e. $-\infty < v_{\parallel\, O^+} < \infty$),

$$G\left(\frac{v}{(2kT_t)/m_t)^{\frac{1}{2}}}\right)=\frac{\Phi\left(\frac{v}{(2kT_t)/m_t)^{\frac{1}{2}}}\right)-\left(\frac{v}{(2kT_t)/m_t)^{\frac{1}{2}}}\right)\frac{\partial}{\partial v}\Phi\left(\frac{v}{(2kT_t)/m_t)^{\frac{1}{2}}}\right)}{2\left(\frac{v^2}{(2kT_t)/m_t}\right)} \qquad (3.26)$$

is the Chandraskhar function.

The H^+ ion is considered to move for a short interval of time Δt, the effect of Coulomb collision at the end of the interval is implemented. To make Δt very small such that the diffusion and friction coefficients do not change during the period we chose Δt to obey equation (2.7). Now the net effect of Coulomb collision during Δt is given by equation (2.6). In order to test the sign of $\Delta v_{\parallel}$ and $\Delta v_{\perp}$, a random variable between (0,1)is generated. If the generated value is <0.5 we pick up the positive sign, otherwise, negative sign will be chosen. Consequently, The H^+ velocities after collision are represented by(*Hinton,* 1983)

$$v'_{\parallel}=(v+\Delta u+\Delta v_{l\parallel})\frac{\Delta v_{\parallel}}{v}-\left(\frac{\Delta v_{\perp}}{\sqrt{2}}\right)\frac{v_{\perp}}{v}$$

$$v'_{\perp}=\left(\left((v+\Delta u+\Delta v_{\parallel})\frac{v_{\perp}}{v}+\left(\frac{\Delta v_{\perp}}{\sqrt{2}}\right)\frac{v_{\parallel}}{v}\right)^2+\frac{(\Delta v_{\perp})^2}{\sqrt{2}}\right)^{\frac{1}{2}} \qquad (3.27)$$

$$v'=\left(v'^2_{\parallel}+v'^2_{\perp}\right)^{\frac{1}{2}}$$

In order to generate a new time step, Δt, we again use $\tau=0.01\,v'/A_s(v')$. The test ion will move in a time Δt under the effect of external forces and Coulomb collision and WPI, and the change in velocities is calculated once again and so on.

3.1.6 The Effect of Wave-Particle Interaction

The wave-particle interaction effect is assumed to affect only the perpendicular velocity of the H^+ ion and the change in velocities due to WPI is given by equation

(2.10). Thus, after the calculation of the change in velocities due to external forces and Coulomb collision we can calculate the change due to WPI, using that equation.

Accordingly, during Δt, H^+ ion moves under the effect of external forces, and the change in the H^+ velocities ($v_\parallel$ and $v_\perp$) can be calculated. This represents the effect of Coulomb collisions and WPI on the H^+ velocities at the end of Δt. Then, another Δt will be generated and we keep computing the H^+ velocities and location until the H^+ ion exits the simulation tube, then another H^+ test ion will be injected into the simulation region.

3.1.7 Calculation of the Distribution Function

The velocity distribution function for the H^+ ions is calculated by using a two dimensional grid in the velocity space ($v_\parallel$, $v_\perp$) to register the behavior of the ion.

The time elapsed by the ion in each bin divided by the bin's volume is proportional to the ion velocity distribution function at the center of the bin. If the bin's volume is $\Delta v^3 = 2\pi\, v_\perp \Delta v_\parallel\, \Delta v_\perp$ and the number of H^+ ions with velocities between v and $v+dv$ is $f(v)d^3v$, then the distribution function of ions is written as: $f(v) = \dfrac{c_2 / |v_\parallel|}{2\pi v_\perp \Delta v_\parallel\, \Delta v_\perp}$, where the numerator comes from the fact that the time needed for the ion to cross the bin is proportional to the width of the bin, which is exactly equal to the width of the bin divided by the parallel velocity. If both sides of the bin are supposed to be equal to $v_{th}/3$, then $\Delta v_\parallel = \Delta v_\perp = v_{th}/3$. In general, the bin volume does not change, but it differs from other bin volume. From this we conclude that $f(v) = \dfrac{c}{|v_\parallel|}$ where c is constant. If $v_\parallel$ and $v_\perp$ are known at a given altitude, the test ion in the corresponding bin can be located

easily. Two integers have been used (J and I) to determine the position of the test ion. Here $J=INT(3\times v_{\perp})$ and because the distribution is symmetric for $v_{\perp}$ around $v_{\parallel}$, J takes the integers from 0 to 10. The J value 10 is taken to be the maximum value of J since it is more than three times the thermal velocity of the background ion, a value that can not be reached by the test ion. Moreover a restriction (J=MIN (J, 10)) has been imposed on J to ensure that we are not sorting outside the array..

According to the parallel direction, the boundaries of the bins are set at (-9.5, -8.5, -7.5, …,7.5, 8.5, 9.5) where the integer I is taken to be $I=NINI(3\times v_{\parallel s})$ between (-10,10).Each bin will be known by (J,I, and altitude). After we have determined the location of the test ion (*i.e.* the bin) we put the numerical value of $f(v)$ in that bin, once another test ion passed that altitude and located into that bin, we added the new numerical value of $f(v)$ to the previous one. We keep doing the above for all test ions.

3.1.8 Moments of the Distribution Function

In this section, we shall determine the moments of distribution function, which include density, drift velocity and parallel and perpendicular temperatures. The test ion distribution function $f_s(v_s)$ is represented by

$$f_s(v_s)=9c_2\sum_i \frac{1}{\left|v^i_{s\parallel\, l}\right|}\frac{\delta\left(v_{s\parallel}-v^i_{s\parallel}\right)\delta\left(v_{s\perp}-v^i_{s\perp}\right)}{2\pi v^i_{s\perp}} \tag{3.28}$$

where $\delta(x)$ is the Dirac delta function. Making use of equation (3.28), the data necessary to compute the velocity moments of the H^+ ion will be accumulated.

3.1.8.1 The Density

The density of bins is defined according to

$$n = \int f(v) d^3v = 2\pi \int f(v) dv_{\parallel} \, v_{\perp} dv_{\perp} \tag{3.29}$$

Substituting *f(v)* from equation (3.28) we get

$$n_i = 9c_2 \sum_i \frac{1}{|v^i_{\parallel}|} \tag{3.30}$$

Thus, the density store $\frac{1}{|v^i_{\parallel}|}$ is added after the location of the test ion has specified.

3.1.8.2 The Drift Velocity

The drift velocity is defined as the expectation value of $v_{\parallel}$ (*i.e.* $\langle v_{\parallel} \rangle$) Thus

$$u = \frac{\int v_{\parallel} \, f(v) d^3v}{\int f(v) d^3v} \tag{3.31}$$

Again, if equation (3.28) is substituted instead of *f(v)* and instead of d^3v, the following expression is obtained

$$u = \frac{\sum_i \frac{v^i_{\parallel}}{|v^i_{\parallel}|}}{\sum_i \frac{1}{|v^i_{\parallel}|}} = \frac{\sum_i sign(v^i{}_{\parallel})}{\sum_i \frac{1}{|v^i_{\parallel}|}} \tag{3.32}$$

3.1.8.3 The Perpendicular Temperature

The random thermal velocity is defined as $\vec{c} = \vec{v} - \vec{u}$. The thermal energy ($\frac{3}{2}kT$) is the expectation value for thermal kinetic energy ($\frac{1}{2}mc^2$) that is

$$\frac{3}{2}kT = \frac{\int \frac{1}{2} m \left[(v_{\parallel} - u)^2 + v^2{}_{\perp} \right] f(v) d^3v}{\int f(v) d^3v} \tag{3.33}$$

or

1) A test H^+ ion is injected into the system at the exobase, *i.e.* random perpendicular and parallel velocities are generated according to equation (3.6) and (3.8) respectively.

2) The H^+ ion is supposed to move for a short period of time Δt under the influence of the external forces, the change in ion's velocity is calculated.

3) The effect of Coulomb collision of H^+ ions with the O^+ background is implemented at the end of Δt using equation (2.6).

4) The effect of wave-particle interaction is also implemented at the end of Δt according to equation (1.6).

5) The H^+ ions are monitored as they cross the predetermined set of altitudes.

6) At each altitude a suitable two-dimensional grid of coordinates parallel and perpendicular to geomagnetic field is used to register the H^+ ion behavior.

7) Steps 1-6 are repeated for 10^5 ions and each time we follow the ion until it exits the simulation region.

8) The accumulative data are used to calculate the velocity distribution function and its moments.

Chapter Four

Results And Discussion

4.1 Introduction

A Monte Carlo technique have been used to study the effects of WPI , coulomb collision and external forces on the H^+ polar wind in the polar cap region from 230 km to 5350 km, a computer code written in FORTRAN language have been used to achieve this purpose. The code works as follows:

1) Divide the simulation region into 22 layers, the gravitational potential is considered to be constant in each layer.
2) Generate randomly the parallel and perpendicular velocities by using a Maxwellian distribution at the bottom of the simulation region.
3) Calculate the time for Coulomb collision.
4) Calculate the time for the particle to cross the upper and lower boundaries of the layer.
5) Follow the particle under the effects of gravity, electric field, divergence of geomagnetic field lines, Coulomb collision and wave-particle interaction.
6) Follow the particle as it moves in the layer and when the particle crosses the upper or lower boundary of the simulation tube, the code accumulates data about the particle distribution function and its moments.
7) Follow the particle until it exits from either top or bottom of the simulation tube.
8) Generate a new particle, the total number of particles is 10^5 particles

4.2 Results And Discussion

4.2.1 The Effect Of WPI (Velocity Independent $\widetilde{D}_{\perp}$)

In the first part of the study the velocity diffusion rate was changed systematically in order to study the effect of constant heating on the H^+ velocity distribution function and its moments.

4.2.1.1 The H^+ Velocity Distribution Function(VDF)

Figure 4 shows the effects of WPI on the H^+ velocity distribution function, the contour levels decrease successively by a factor of $e^{1/2}$ from the maximum. At the exobase (230 km), the H^+ distribution function, $f(H^+)$, is non-drifting Maxwellian, this is consistent with the assumption at the lower boundary.

Comparing the first panel to the left of Figure 4 (left, $\widetilde{D}_{\perp} = 0$) with the results of *Barakat et al.*, 1995, which neglects the effects of WPI, we can see that we have reproduced the same results. At the exobase the distribution function is very close to Maxwellian and as the ions drift upward to higher altitudes, the high speed ions are accelerated upward by the body forces, while the low-speed ions remain coupled to the O^+ ions. Hence, $f(H^+)$ forms an upward tail, as shown in the first panel of Figure 4 $\widetilde{D}_{\perp} = 0$ at altitude 890 km. As the H^+ ions reaches even higher altitudes, the high-speed portion of $f(H^+)$ is further accelerated upward while the low-speed portion remains coupled to the O^+ ions, this leads to the double hump shape for the VDF.

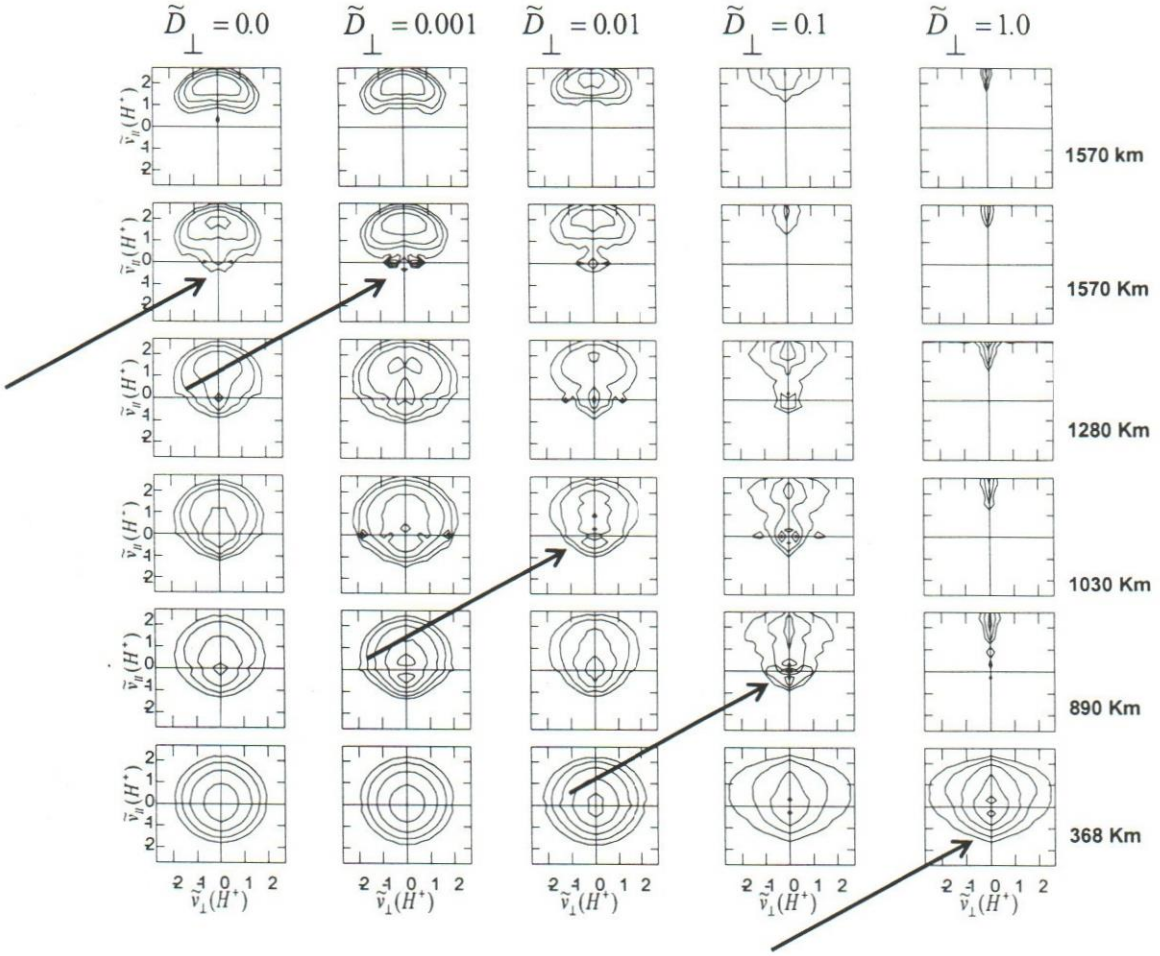

Figure 4: H^+ velocity distribution function in the case of velocity-independent WPI for five WPI levels=0, 0.001, 0.01, 0.1 and 1.0. and for 6 different altitudes: 368 km, 890 km, 1030 km, 1280 km, 1570 km and 1850 km. $f(H^+)$ is represented by the equal-valued contours in the normalized velocity.

The high-speed portion of $f(H^+)$ grows rapidly with altitude, while the low-speed portion diminishes. We can notice also that the low-speed portion vanishes at altitude 1850 when no WPI, and $f(H^+)$ takes the 'Kidney bean' shape characteristics of the high-speed portion. At high altitudes, $f(H^+)$ changes again from double-hump to become close to a bi-Maxwellian shape. The bi-Maxwellian shape appears as a result of the geomagnetic field, while the kidney bean shape appears since the perpendicular

Coulomb collision diffusion rate is much greater than the parallel one for the high-speed ions.

Let us now see what happened to $f(H^+)$ when we add the effect of WPI. As mentioned before, at the exobase (230 km) the distribution function is not affected by the WPI, this is consistent with the assumption about the velocity distribution function of the injected ion at the lower boundary. The WPI heats the ions in the perpendicular direction, this increases the upward mirror force and hence accelerates the H^+ ions in the parallel direction.

The WPI and Coulomb collision together increase the velocity of the high-energy particles, because these ions are heated due to WPI and are less coupled with the O^+ background, hence they escape into the upward direction. This explains the high-velocities observed as $D_\perp$ increases at constant altitude. At low altitudes, and as $D_\perp$ increases the width of $f(H^+)$ increases and consequently, the temperature anisotropy decreases (i.e. $T_\perp < T_\parallel$).

Since the WPI increases the velocity of the high-speed ions, the double –hump distribution predicted by *Barakat et al.*, 1995 appeared at lower altitudes. At large WPI levels ($D_\perp$ =0.1 and 1.0) the effect of WPI has become the dominant factor and most of the ions have become less coupled with the O^+ background. Therefore, they easily escape in the upward direction

4.2.1.2 Moments of H+ Distribution

Figure 5 shows the profiles of H^+ density, drift velocity, parallel temperature and perpendicular temperature. As WPI strength increases, the drift velocity increases especially at high altitudes, which can be explained as follows: the WPI heat the ions in

the perpendicular direction, which increases the upward mirror force and hence, accelerates the H^+ ions in the upward direction. Since the H^+ ions are in flow-limiting flux condition $\tilde{n}\tilde{u} = 1$ (*Barakat and Schunk*, 1983) a corresponding decrease in the H^+ density (top left panel) is expected in order to keep the net escape flux constant.

The behaviour of the perpendicular temperature (bottom left panel) is a result of the balance between the heating due to WPI and the perpendicular adiabatic cooling. On one hand, at low altitude the WPI is dominant, and the perpendicular temperature is increased. On the other hand, the perpendicular temperature decreases at high altitudes due to perpendicular adiabatic cooling which is the dominant effect there. As the strength of WPI increases (i.e. $\tilde{D}_\perp$ increases) the perpendicular temperature increases as a result of heating in the perpendicular direction. The profiles of H^+ parallel temperature are shown in the bottom right panel of Figure 5. The WPI has a two-fold effect on the parallel temperature. First, the increase in upward mirror force results in parallel adiabatic cooling. Second, the transfer of energy from the perpendicular to the parallel direction enhances the parallel temperature. As a result of the interplay between the two factors, the parallel temperature first increases due to the second effect (energy transfer from the perpendicular to the parallel directions), but at high altitudes, the first effect (enhanced parallel adiabatic cooling) is dominant. For large WPI levels ($\tilde{D}_\perp$ =1.0, 5.0 and 10.0) we can notice that the parallel temperature is increasing always which means that the second effect is always dominant for large WPI levels

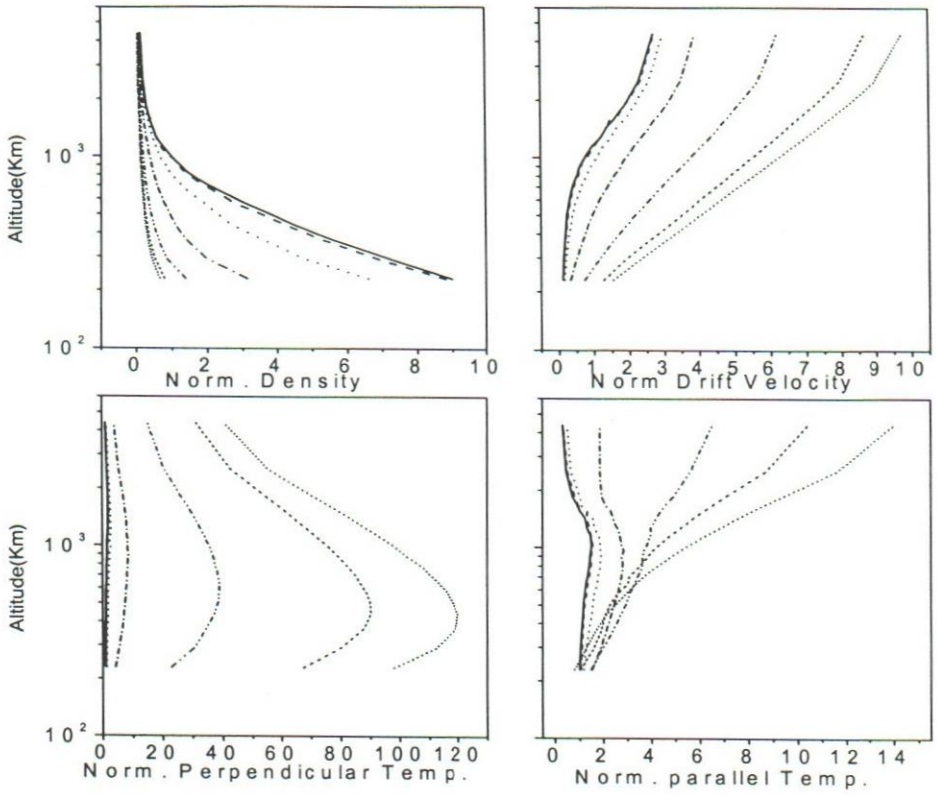

Figure 5 Altitude profiles for the different H^+ moments for different values of $\widetilde{D}_\perp$: $\widetilde{D}_\perp$=0 (solid), $\widetilde{D}_\perp$=0.001(dashed), $\widetilde{D}_\perp$=0.01(dotted), $\widetilde{D}_\perp$=0.1(dashed-dotted), $\widetilde{D}_\perp$=1.0(dashed-dotted-dotted), $\widetilde{D}_\perp$=5.0(short-dashed), $\widetilde{D}_\perp$= 10(short dotted). The moments considered are density, drift velocity, and parallel and perpendicular temperatures.

4.2.2 The Effect Of WPI (Velocity-Dependent $\widetilde{D}_\perp$)

In this section we report the effects of velocity-dependent WPI on H^+ velocity distribution function and its velocity moments, where the modified form of the diffusion rate $\widetilde{D}_\perp$ has been used.

4.2.2.1 The H+ Velocity Distribution Function (VDF).

Figure 6, exhibits a comparison between the effects of velocity-dependent WPI (right panel) and velocity-independent WPI (left panel) for $\widetilde{D}_{\perp}$=0.001. Both panels have shown similar behaviour for H^{+} velocity-distribution, because the effect of WPI is negligible. The double-hump distributions are well pronounce in the left panel of Figure 7 for $\widetilde{D}_{\perp}$=0.01, however as a result of velocity-dependent WPI, the strength of heating decreases and hence the formation of the double-hump disappeared. Similarly, the double-hump distributions for the case $\widetilde{D}_{\perp}$=0.1 (Figure 8) are well pronounce for the velocity-independent WPI (left panel). However, for the case of velocity-independent WPI (right panel), the double-hump distribution did not appear. This is due to the effect of velocity-dependent WPI which on turn decreases the level of heating and then, the number of H^{+} ions that are less coupled with the background decreases. Therefore, the secondary peak did now appear.

In the case where $\widetilde{D}_{\perp}$ =1.0 (Figures 9) and generally high WPI levels, we can notice that for the case of velocity-independent WPI most of the particles escape from the simulation region especially at high altitudes, due to high level of WPI ,however, for the case of velocity-dependent WPI the level of WPI becomes moderate.

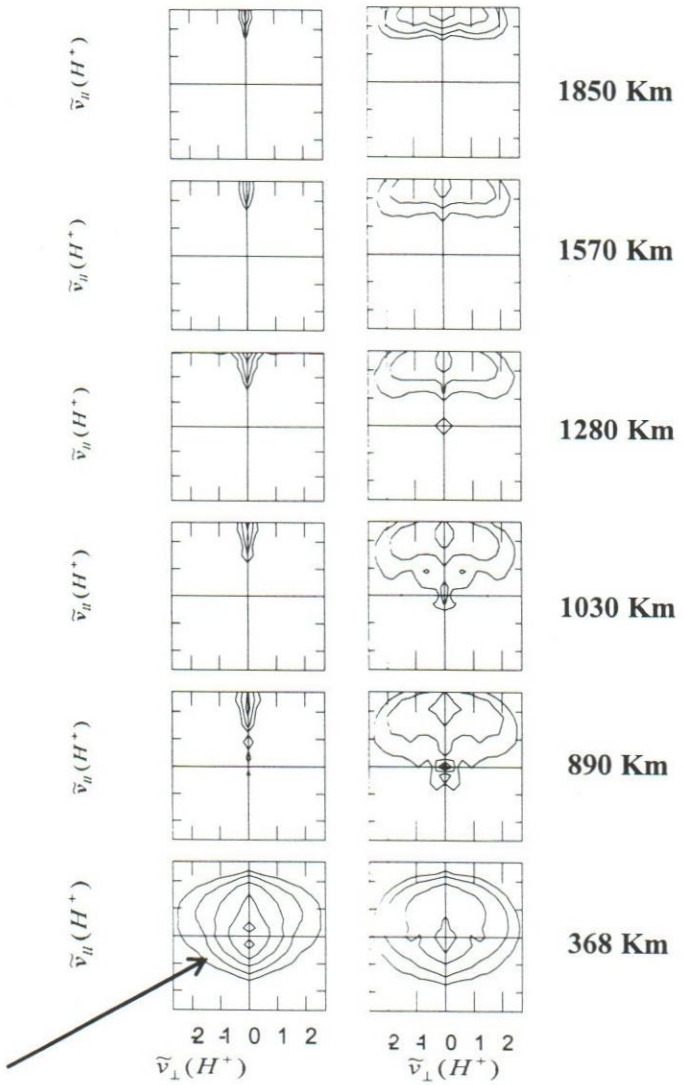

Figure 9: Comparison between The H^+ velocity distribution function for two cases : the velocity independent (left column) and the velocity dependent (right column) wave particle interaction for the case of $\tilde{D}_\perp$=1.0 and for 6 different altitudes.

4.2.2.2

Moments of H+ Distribution

Figures 10-14 show the H^+ moments for velocity-independent WPI (solid) and velocity-dependent WPI (dashed) for different values of $\tilde{D}_\perp$. The difference in the

behaviour of the H^+ moments for the case of $\tilde{D}_\perp$=0.001 is negligible. This is in agreement with the results obtained for the distribution function (Figure 6), because the level of heating is negligible. Therefore, both cases velocity-dependent and velocity-independent WPI produce similar behaviours. However, as $\tilde{D}_\perp$ increases, the differences between the corresponding H^+ moments become well pronounced.

The drift velocity, parallel temperature and perpendicular temperature are shifted toward lower values for velocity-dependent WPI. However, the H^+ density is shifted toward higher values for velocity-dependent WPI, and this is due to limiting flux tube effect $\tilde{n}\tilde{u} = 1$.

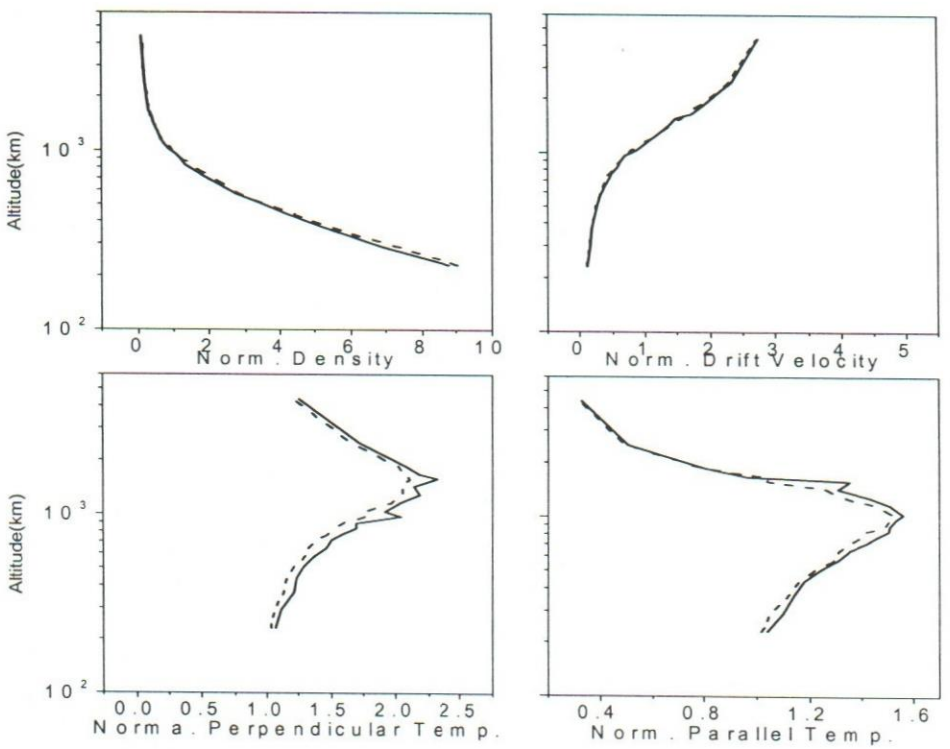

Figure 10: Comparison between the parametric study(solid)and the velocity dependent study (dashed) for the case $\tilde{D}_\perp$=0.001 . The moments considered are density, drift velocity, parallel temperature and perpendicular temperature.

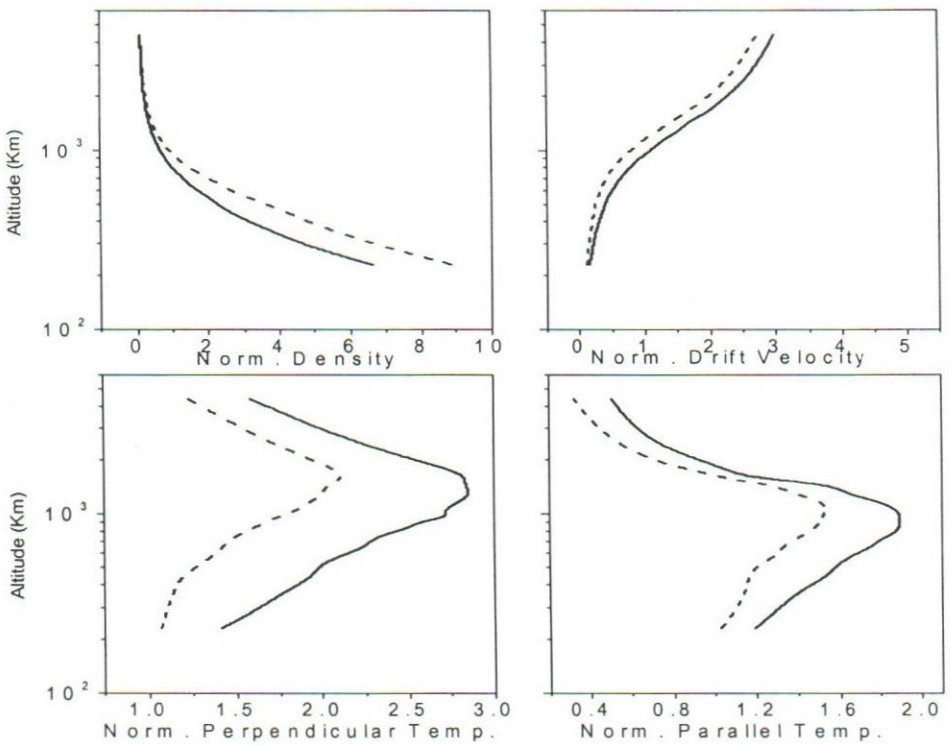

Figure 11: Comparison between the parametric study(solid)and the velocity dependent study (dashed) for the case $\widetilde{D}_{\perp}$=0.01 . The moments considered are density, drift velocity, parallel temperature and perpendicular temperature.

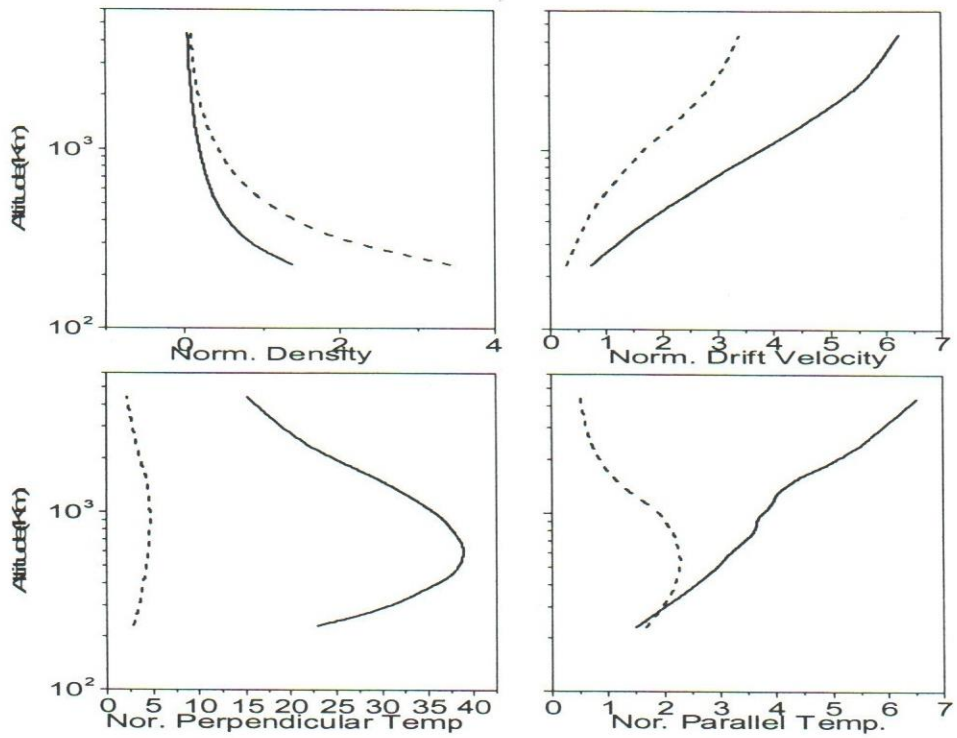

Figure 13: Comparison between the parametric study(solid)and the velocity dependent study (dashed) for the case $\widetilde{D}_{\perp}$=1.0 . The moments considered are density, drift velocity, parallel temperature and perpendicular temperature.

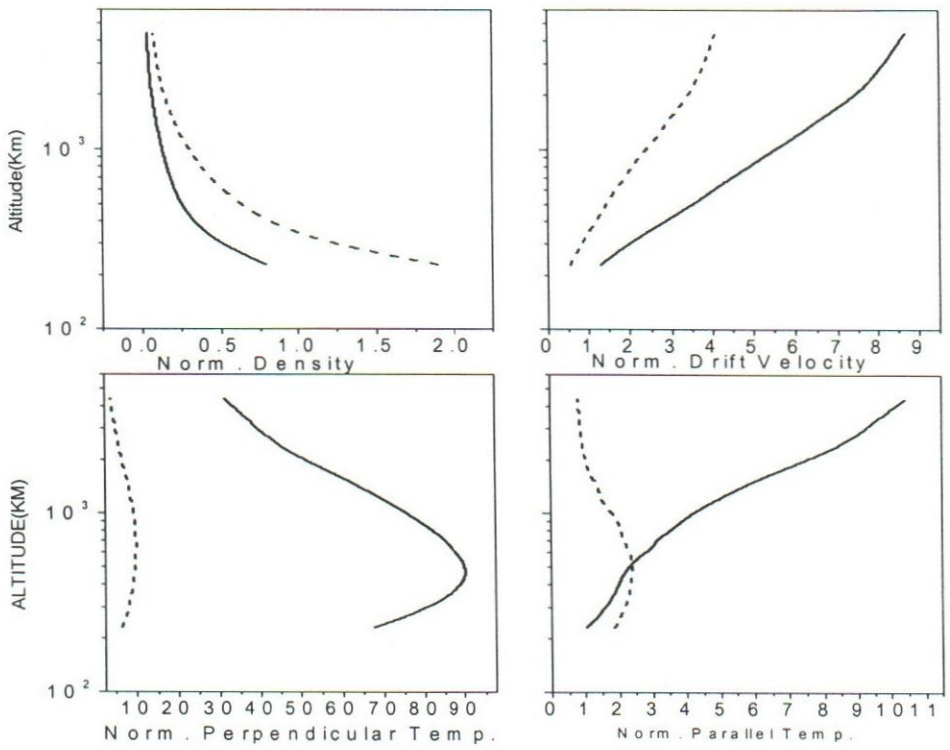

Figure 14: Comparison between the parametric study (solid)and the velocity dependent study (dashed) for the case $\widetilde{D}_{\perp}$=5.0 . The moments considered are density, drift velocity, parallel temperature and perpendicular temperature.

Chapter Five

CONCLUSION AND FUTURE WORK

Chapter Five

Conclusion And Future Work

5.1 Conclusion

The Monte Carlo simulation was used to study the effects of WPI, Coulomb collision, gravity, polarization electric field and geomagnetic field on the H^+ polar wind from 230 Km to 5350 Km above the polar cap region. The H^+ velocity distribution function and its moments were calculated, our main conclusion is that WPI has a great influence on the characteristics of the H^+ polar wind as follows:

1) WPI accelerates the ions leading to a modification on the VDF.

2) WPI keeps the double-hump velocity distribution function discovered by *Barakat et al.*, (1995).

3) The density of H^+ is decreased as a result of WPI especially at low altitudes.

4) WPI enhances the drift velocity of the H^+ ions especially at high altitudes.

5) The perpendicular temperature increases as the strength of WPI increases especially at 400 Km.

6) WPI enhances the parallel temperature.

7) The inclusion velocity dependent WPI decrease the effect of WPI.

Schunk, R. W., and D. S. Watkins, (1981), *J. Geophys. Res.*, **86**,91.

Schunk, R. W., (1977), *Rev. Geophys.*, **15**,429.